JOURNAL OF THE KOREAN ASTRONOMICAL SOCIETY
27: 159 ~ 175, 1994

A STUDY OF LYNDS 1251 DARK CLOUD: I. STRUCTURE AND KINEMATICS

LEE, YOUNGUNG
Korea Astronomy Observatory, Taejon, Korea
(Received Sep. 23, 1994; Accepted Oct. 17, 1994)

ABSTRACT

We have mapped the whole extent of a dark cloud Lynds 1251 in the emission of the $J = 1 - 0$ transitions of ^{12}CO and ^{13}CO using FCRAO's fifteen-beam array receiver in high angular resolution of $50''$. We have derived physical parameters of L1251, discussed three different mass estimate techniques, and obtained a large range of mass, 600 to 6,000 $M_\odot$, depending on the techniques. The factor of 10 discrepancy between the virial and LTE masses is much larger than expected based on the uncertainties residing in two methods. The large virial mass may reflect the fact that L1251 is not gravitationally bound system as in the case of dark clouds in solar neighborhood. Two outflows are affecting the dynamics of cloud significantly but not enough to reshape the whole extent of the cloud. The small cloud, 'Stripe', which is apparently connected with main cloud, is not likely to be associated with L1251. The velocity gradient composed on this small cloud may be driven by other unknown sources. It is found that L1251 cloud itself is very quiescent except the two bipolar outflow regions.

I. INTRODUCTION

A small elongated dark cloud L1251 is located in the constellation of Cepheus ($\alpha = 22^h35^m$, $\delta = +75°0'$), which is probably a part of more extended molecular complex, known as 'Cepheus Flare' (Grenier *et al.* 1989). L1251 has been classified as high-opacity cloud (opacity class 5 in the Lynds catalog, 1962), and is distinct on the Palomar Observatory Sky Survey (POSS) print. L1251 is located fairly far above the Galactic plane, $b \simeq 15°$, thus it is implicit that there is little contamination with gas in Galactic plane. Several small clouds are existent around L1251. The closest one is L1247, located in the western part of the cloud. In addition to L1247, there is one small dark clouds associated, KHAV776. LBN558 (Lynds Bright Nebula Catalog; Lynds 1965) is also associated with the southern part of the cloud on the POSS overlay. A spiral galaxy, UGC 12160, is located on the edge of the cloud. However, this is a very distant object, thus it does not affect any results on CO observations of L1251. Toward L1251 there are many IRAS point sources and Hα emitting stars (Kun and Prusti 1993), which is the sign of recent star formation. One bright late-type star (SAO10440, spectral type K5) is located on the IRAS point source IRAS 22361+7506.

Grenier *et al.* (1989) have mapped in CO $J = 1 - 0$ the very large region including L1251 and L1247 with a resolution of half degree, and claimed that the region is currently being exposed to an external shock probably generated by a supernova. Sato and Fukui (1989, 1994) studied L1251 mainly on the star forming activities and density structure. Fuller (1989) reported a slight velocity gradient across the dense core in the head of L1251, and Sato and Fukui (1994) claimed a highly ordered velocity gradient toward the direction of head part of the cloud. They interpreted this gradient caused by interaction with unidentified ambient matter.

In this paper, with a high angular resolution mapped data set, we derive physical parameters and discuss dynamics of the cloud. The heating of gas and dust (FIR properties) will be discussed in a separate paper (Lee 1994a; Paper II).

II. OBSERVATIONS

We have mapped the whole region of L1251 and part of L1247 in the transitions of ^{12}CO and ^{13}CO $J = 1 - 0$ using the QUARRY fifteen-beam array receiver at the FCRAO 14 m radio telescope (FWHM = 47″) between 1993 February and May. The spectra were spaced by 50″, and covered 100′ × 45′ region. ^{12}CO map consists of 6,750 spectra, and ^{13}CO map consists of 5,940 spectra. Two filterbanks with thirty-two channels each having frequency resolutions of 250 KHz and 1 MHz were used for each beam. A velocity coverage of 21 km s^{-1} and resolution of 0.65 km s^{-1} is therefore provided with the 250 KHz filterbank at the frequency of the $J = 1 - 0$ line. The 1 MHz filterbank provided a velocity coverage of 85 km s^{-1} with a resolution of 2.6 km s^{-1}, and was used to check if emission at other velocities was detectable toward the cloud.

All observations were made by repeatedly switching to one reference position at $\alpha = 22^h30^m$, and $\delta = 75°30'$ confirmed to have no CO emission. Each reference observation was shared with observations at 4 to 6 map positions depending on the sky stability. Calibration was accomplished by frequently observing an ambient temperature load. All antenna temperatures quoted are corrected for atmospheric extinction and for the forward spillover and scattering losses of the antenna and radome ($\eta_{fss} = 0.7$ at 110 to 115 GHz), and are therefore on the T_R^* temperature scale defined by Kutner and Ulich (1981).

Additional observation in high sensitivity toward $\alpha = 22^h27^m29^s.4, b = 74°50'$ was made to check the possible association of two superposed clouds (see §3) in the transition of ^{12}CO J = 1-0 using Daeduk Radio Astronomy Observatory (DRAO) 14 m telescope. Two filterbanks with 256 channels having a frequency resolution of 250 KHz were used. All observations were made by repeatedly switching to the same reference position as above. Calibration was accomplished by frequently observing an ambient temperature load. All antenna temperatures quoted are corrected for atmospheric extinction and for the forward spillover and scattering losses of the antenna and radome ($\eta_{fss} = 0.68$ at 115 GHz), and are therefore on the T_R^* temperature scale. The rms noise for this observation is 0.03 K.

III. RESULTS

(a) Cloud Morphology and Velocity Structure

The ^{12}CO integrated intensity map of L1251 is presented in Figure 1 in grey scale. The overlayed contours are representing far-infrared flux at 100 μm. L1251 has an extent of 1°.5 in Right Ascension direction and 0°.8 in Declination direction. Assuming a distance of 300 pc given by Kun and Prusti (1993), the full extent of the cloud is 8 pc ×4.2 pc. The morphology of L1251 is characterized by elongated cigar-like shape. The more intense emission at the western part of cloud is from L1247, a nearby cloud. The ^{12}CO emission drops relatively sharply in the eastern part, and it is extended to L1247 in the western part. Comparison with the POSS print indicates that the molecular gas distribution is well matching with the visual extinction distribution. The boundary of ^{12}CO emission is almost perfectly matching with the lowest contour level of 100 μm flux, which confirms that there is little gas and dust in the foreground or background. It is likely that the FIR emission is totally coming from L1251.

The ^{12}CO peak temperature of the cloud is 5.8 K, and the ^{13}CO peak temperature is 4.7 K. The ^{13}CO peak temperature map is presented in Figure 2 with the same contour map overlayed as in Figure 1. In pixel-to-pixel plot (Figure 3) between ^{12}CO and ^{13}CO peak temperatures a correlation can be found. All the pixels toward the cloud above ^{12}CO peak temperature greater than 1 K are entered. The average peak temperature ratio between two isotope (T (^{12}CO) > 2.5 K) is ~ 0.4. This ratio is very high for a dark cloud. Typical average value of dark clouds is less than 0.2 (Sanders *et al.* 1993). Thus, L1251 can be categorized as a very opaque cloud. The fact that the cloud is highly opaque (optically thick) can also be confirmed by comparing its spectra with other cloud's spectra. Figure 4 shows averaged spectra of the whole extent of L1251 and L1247 included within our map range, respectively. The ^{13}CO temperatures distribution of two clouds are quite different: the ^{13}CO temperature of L1251 is a factor of three higher than that of L1247.

One interesting fact is that the ^{12}CO linewidths found in L1247 (ΔV is ~ 5 km s^{-1}) are much broader than typical linewidths found in normal dark cloud (ΔV ~ 2 to 3 km s^{-1}) and our main cloud L1251 (~ 3 km s^{-1}). More study on L1247 remains to be done.

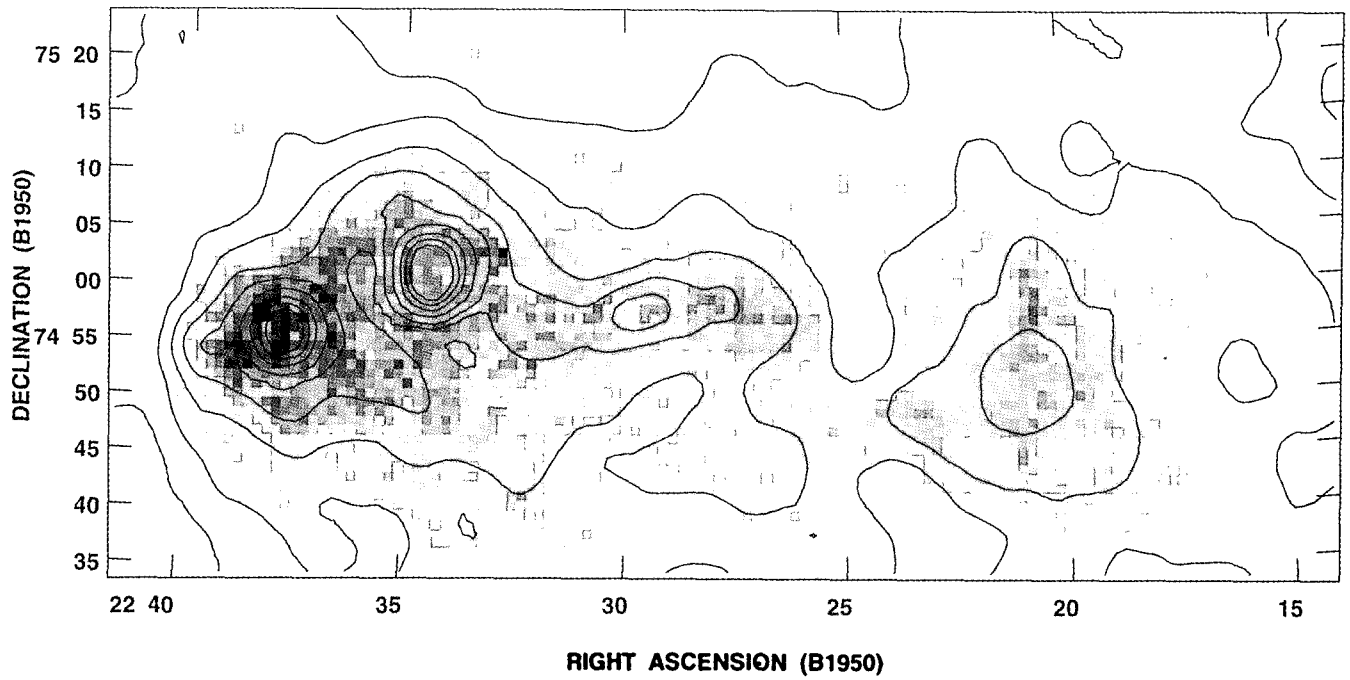

Fig. 1. The ^{12}CO integrated intensity grey-scaled map of L1251 dark cloud. The IRAS flux contour map at 100 μm is superposed on the grey-scaled map. The contour levels are 20, 40,60,80, 100, 140, 200, 260, 320 ... MJy/sr. The grey scale ranges from 1.5 to 18 K km s^{-1}.

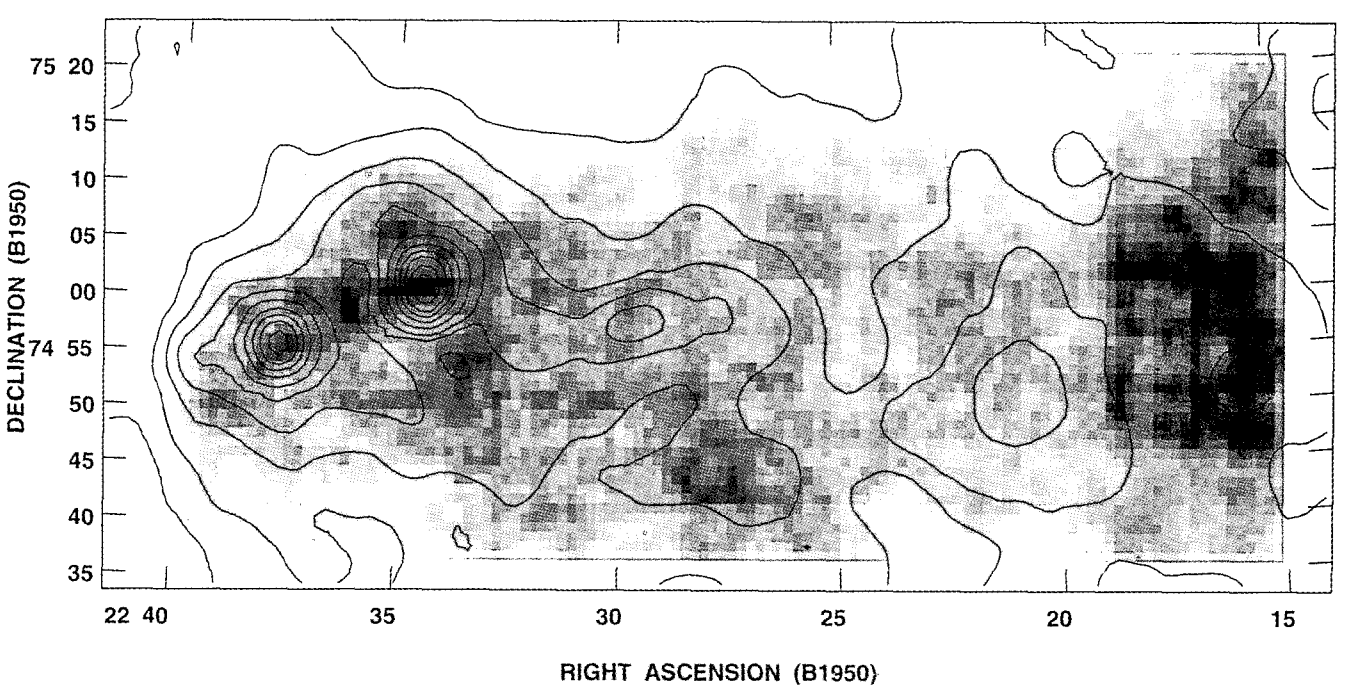

Fig. 2. The ^{13}CO peak temperature grey-scaled map of L1251 dark cloud. The superposed contours are the same as in Figure 1. The grey scale ranges from 0.6 to 4 K.

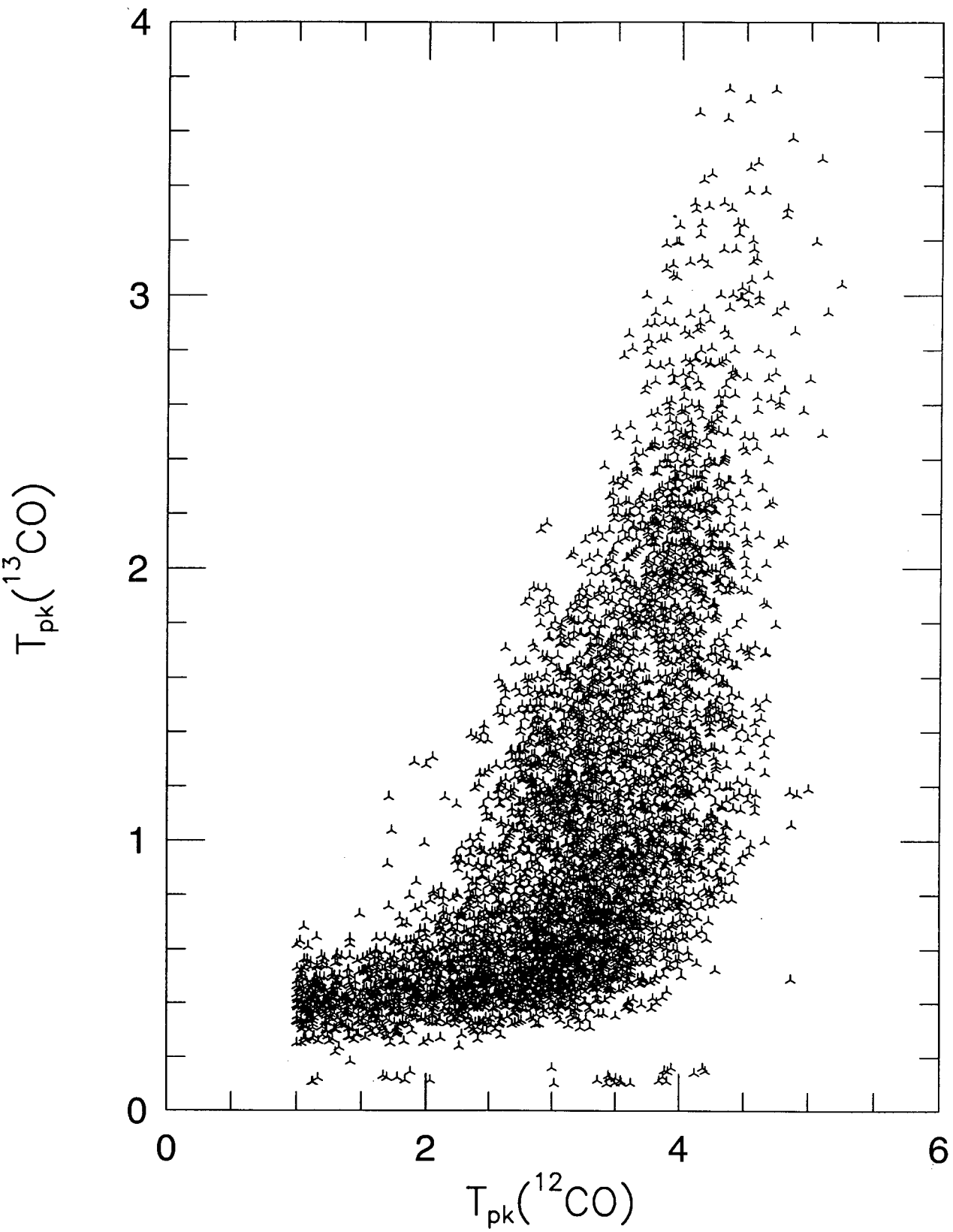

Fig. 3.. The ^{12}CO peak temperature versus ^{13}CO peak temperature plot for the all pixels of the cloud with ^{12}CO peak temperature larger than 1 K.

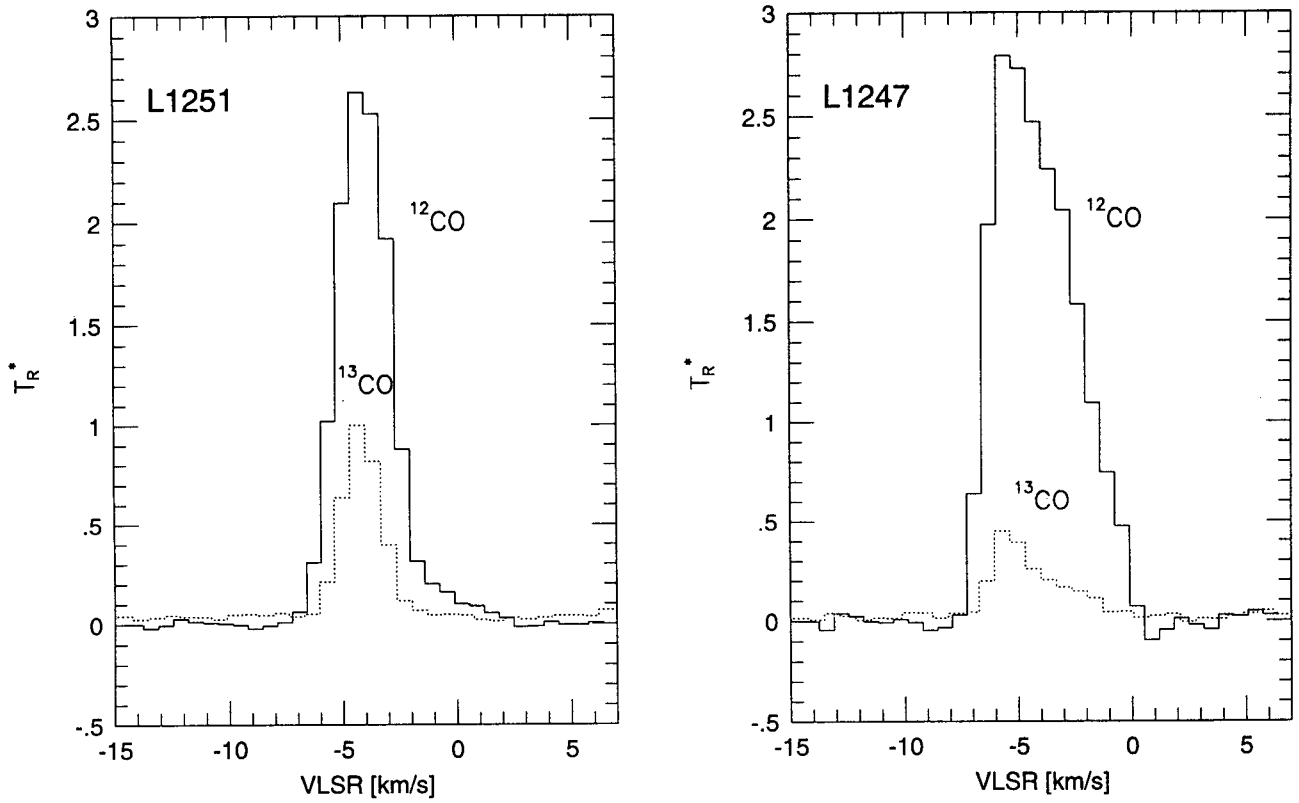

Fig. 4. Averaged ^{12}CO and ^{13}CO spectra of L1251 and L1247. The linewidths of L1247 is much broader than than of L1251.

Maps at individual velocities are shown in Figure 5. The velocity coverage of each map is 0.65 km s^{-1}, which is corresponding to one channel of 250 KHz filterbank. The covered velocity range is -7.58 to $+2.18$ km s^{-1}. The ^{12}CO emission actually arises from -9 km s^{-1}, but not included in this map. Considering the mean velocity of the cloud, -3.9 km s^{-1}, the velocity range of L1251 is very large. In fact, the emission arising centered at $\alpha = 22^h35^m, \delta = 75°$ is a bipolar outflow, which is also matching with IRAS point source 22343+7501. There is another smaller bipolar outflow, matching with IRAS point source 22376+7455. Sato and Fukui (1989) also reported these two bipolar outflows. More discussion on the bipolar outflows will follow in next section. The low-velocity region seems to be dominated by emission of a bipolar outflow 22343+7501, and in higher velocity region, ^{12}CO emission is more spreaded over the whole extent of the cloud. In more higher-velocity region, there is conspicuously stripe-like emission (hereafter we call it 'Stripe'), which is running from upper left to lower right direction at the velocity frame of -0.42 km s^{-1}. The 'Stripe' feature is very interesting for this kind of molecular cloud though the emission is weaker than the major part of the cloud. The possibility of association with main cloud will be discussed in later section.

In Figure 6 we present a series of Right Ascension-velocity maps at all the declination position with 50″ spacing and with the velocity range of -14 to $+6$ km s^{-1}. The first frame is corresponding to $\delta = 74°34'$ (Frame number 1) and the last one (Frame number 60) is $\delta = 75°24'$. The 'Stripe' feature is more conspicuous at the frames 4 to 19. The velocity range of the 'Stripe' is extended more than 5 km s^{-1}, and the emission is apparently connected with the main cloud. The velocity ranges of bipolar outflow 22343+7501 and 22376+7455 can be seen from frames 30 to 44 centered on $\alpha = 22^h34^m$. It can be notified that the velocity range of adjacent cloud L1247 is much broader than that of L1251 as mentioned above.

A position-velocity map is presented in Figure 7, which cuts the whole cloud along the declination (horizontally). This map also shows that there is a conspicuous 'Stripe's velocity component. While the main cloud shows little velocity gradient, the 'Stripe' shows clear velocity gradient. The emission of the main cloud is confined at the velocity of -4 km s^{-1}. The velocity difference between the main cloud and the 'Stripe' along this direction is ~ 5

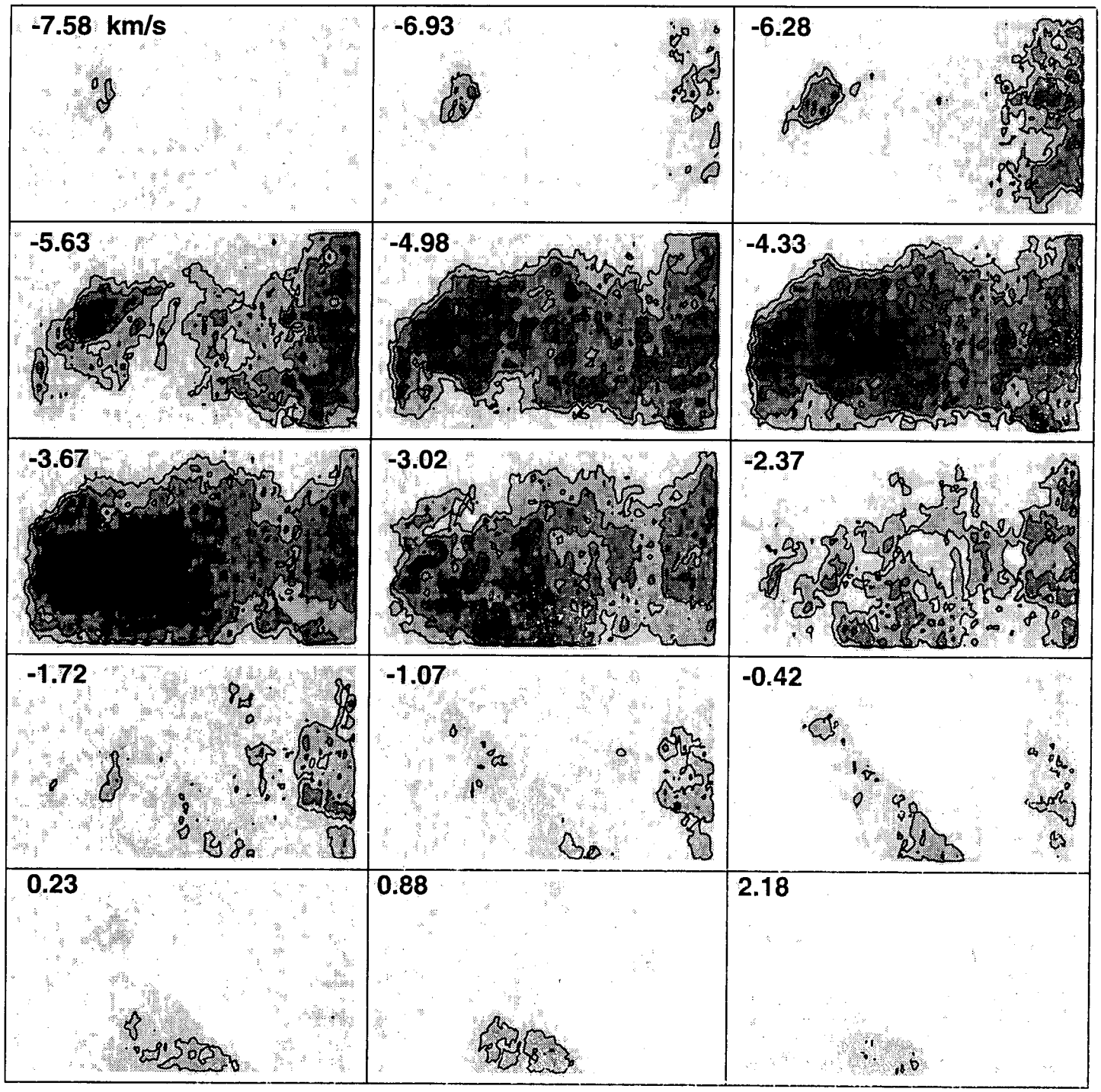

Fig. 5. The ^{12}CO velocity maps of L1251. Each map has V_{LSR} range of 0.65 km s^{-1}, which is corresponding to one channel of 250 KHz spectrometer. The centered velocity of each map is marked at the upper-right corner. The contour levels are 0.7, 1.75, and 2.8 K. The grey scale ranges from 0.3 to 4.5 K.

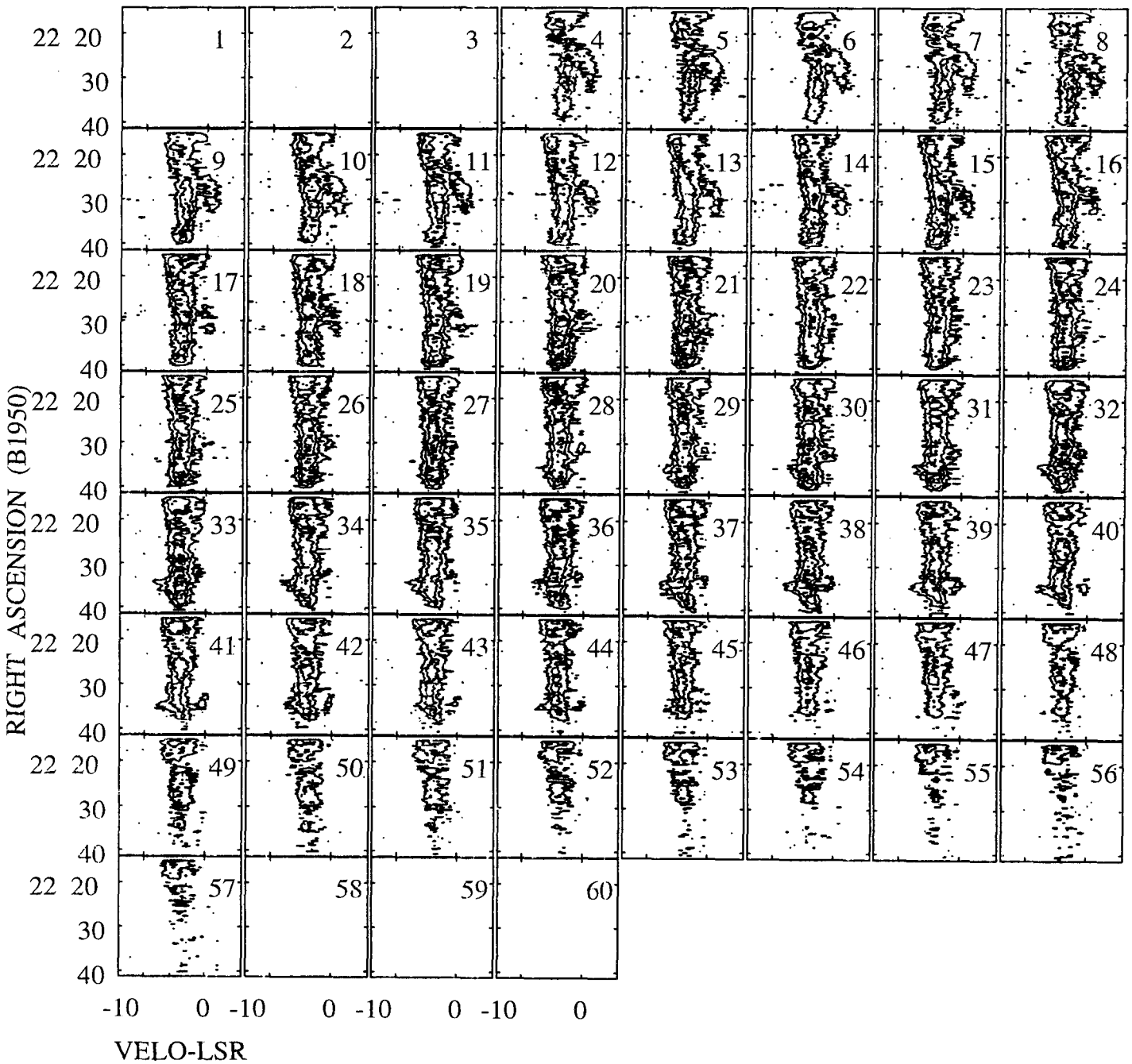

Fig. 6. Series of Right Ascension-velocity maps (^{12}CO) at all the declination position with $50''$ spacing and with the velocity range of -14 to 6 km s^{-1}. The first frame is corresponding to $\delta = 74°34'$ (Frame number 1) and the last one (Frame number 60) is $\delta = 75°24'$. Note the velocity range of the 'Stripe', and that it is apparently connected with the main cloud. The contour levels are 0.7, 2.5, and 4.5 K.

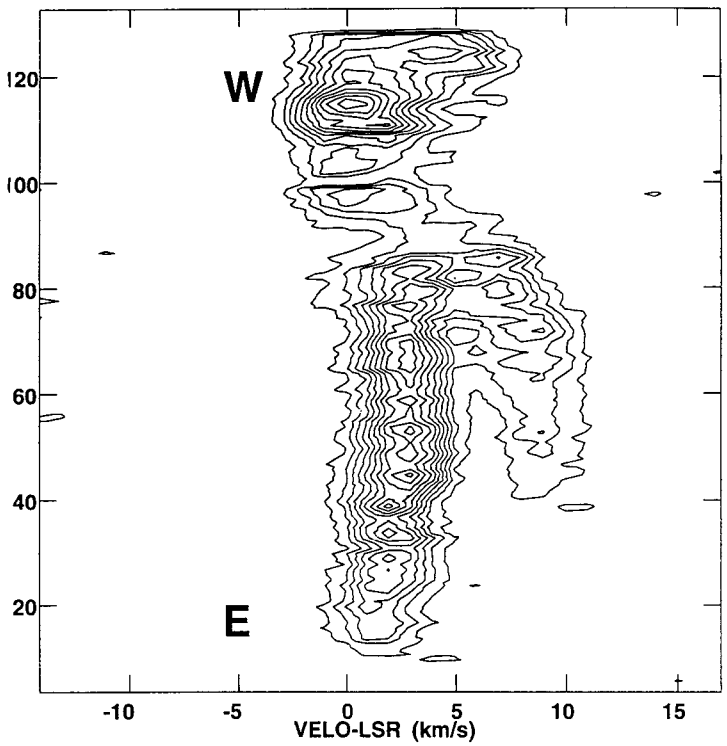

Fig. 7. A ^{12}CO position-velocity map for the cut of the main body of the cloud along the declination. The Distance axis is in the unit of pixel size, $50''$, thus the whole length of the cut is $\sim$ 2 degrees. Note that the 'Stripe' cloud is elongated at the velocity range from -1 to $+2$ km s^{-1}. The lowest contour is 1 K, and the increment between the contours is 1.2 K.

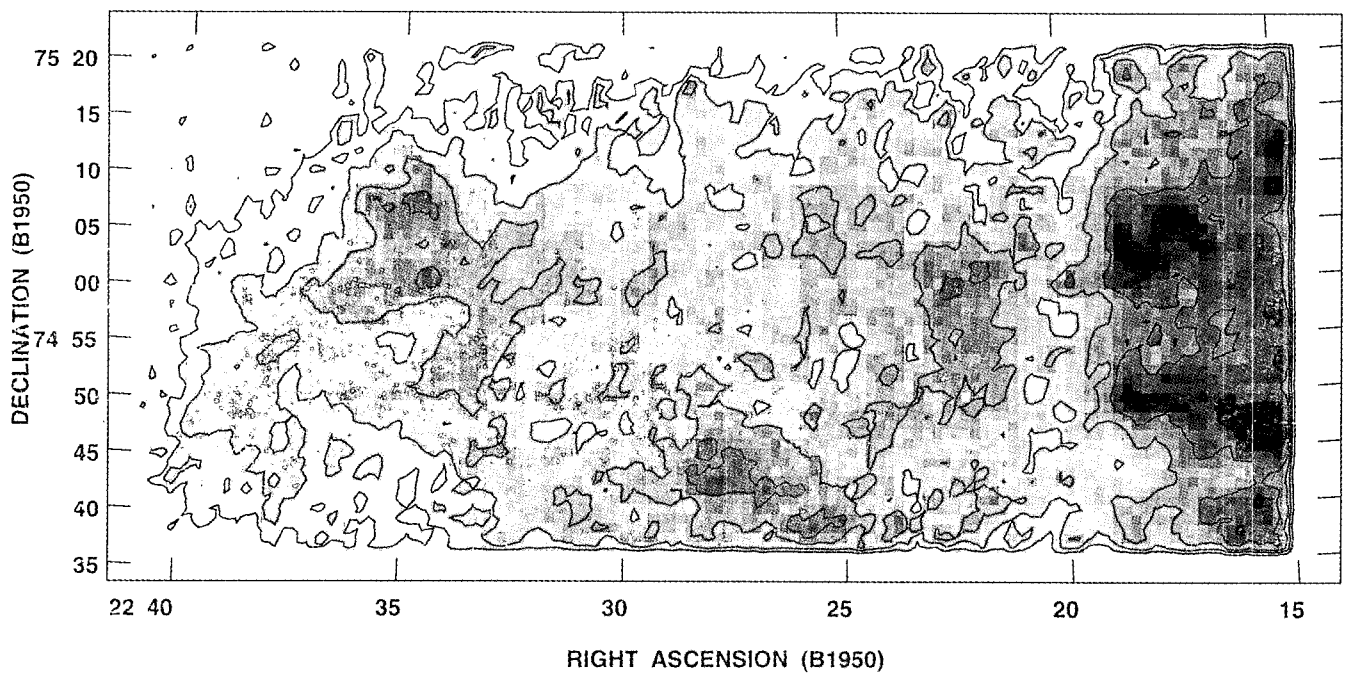

Fig. 8. Mean ^{12}CO velocity map of L1251. The mean velocity is computed only for the regions where the ^{12}CO integrated intensity is greater than 5σ of the noise. Darker color represents higher velocities (blue), and the lowest contour level is -6 km s^{-1} and the increment is 0.75 km s^{-1}.

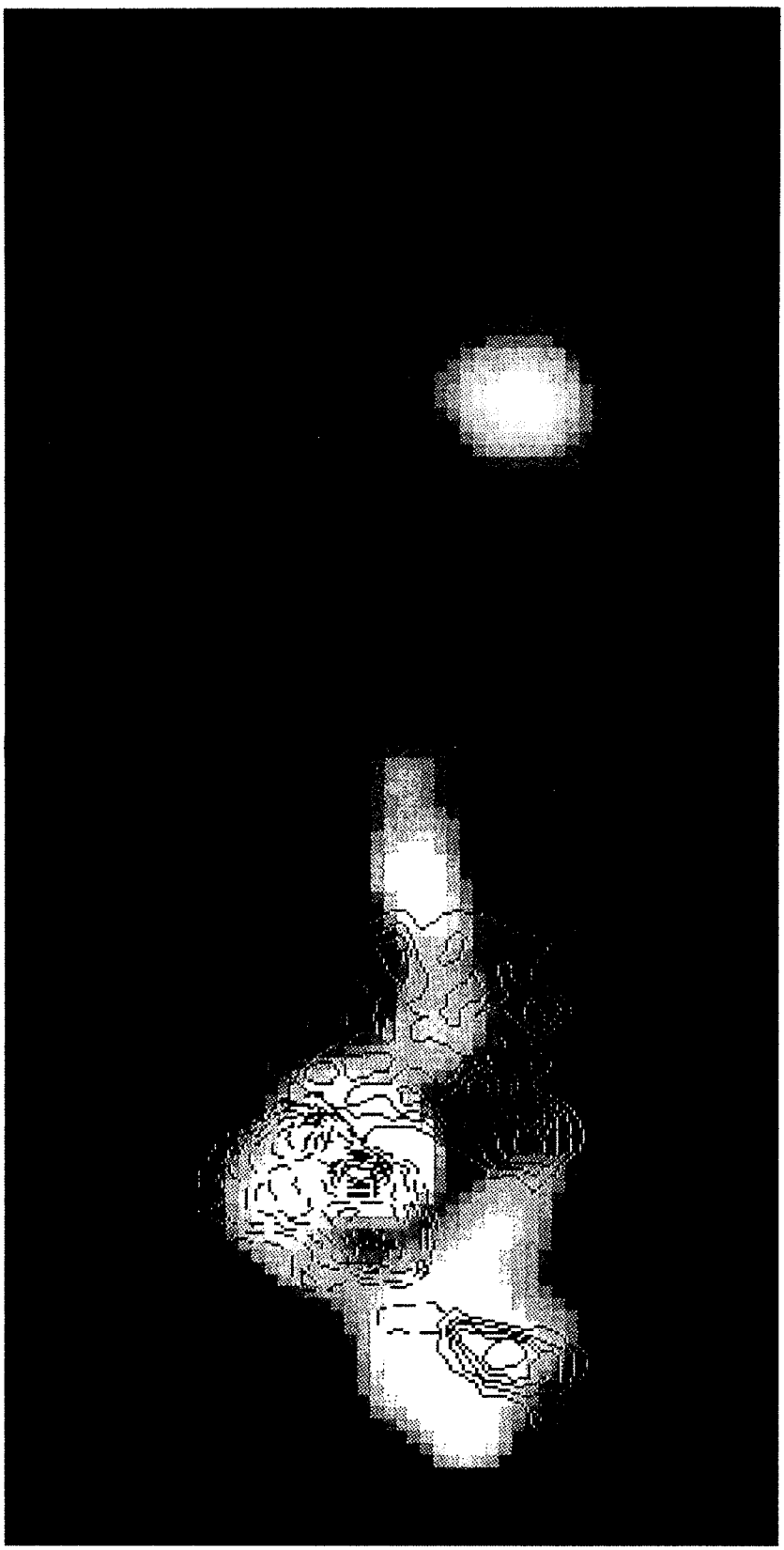

Fig. 9. The contour maps of two bipolar outflows superposed on the 100 μm flux image. Dashed contour lines represent red wing, and solid one is blue wing (see text). Smaller and well collimated one is outflow A, and the larger and more extended one is outflow B. The bright color represents more higher flux in the color image. The lowest contour and the increment between the contours are 0.4 K, respectively.

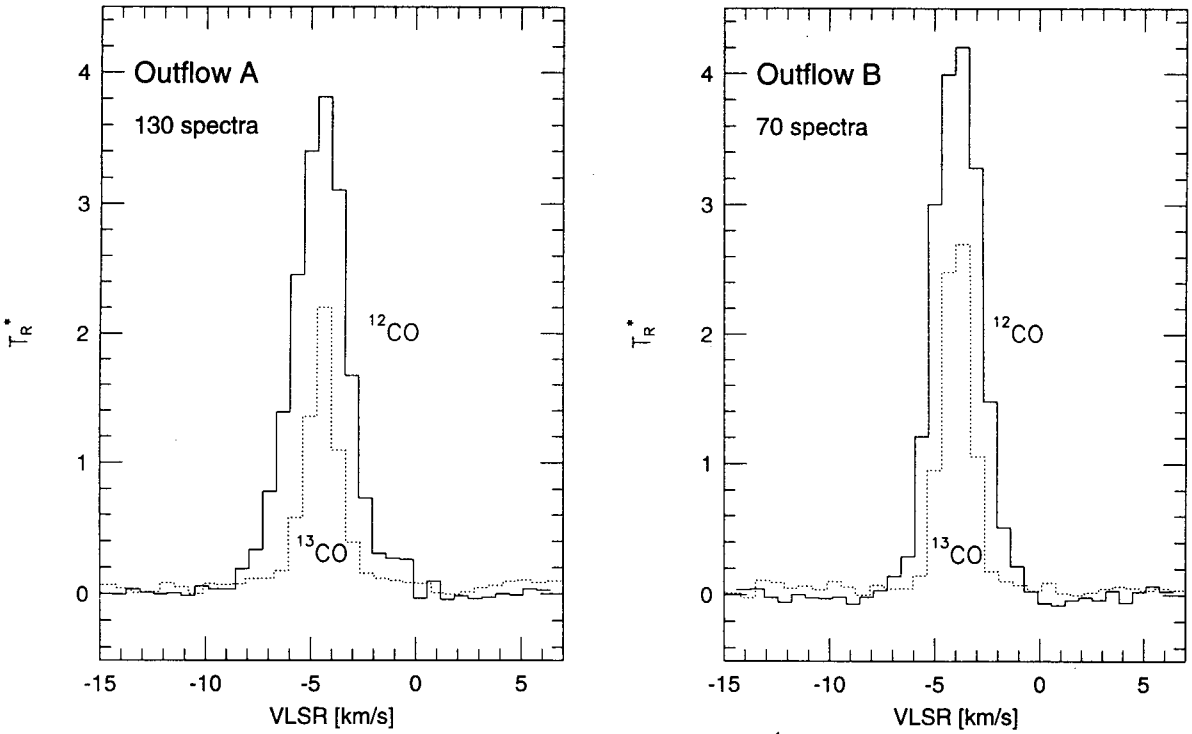

Fig.10. Averaged profiles centered on two bipolar outflows. One hundred and thirty (^{12}CO and ^{13}CO each) spectra were averaged toward Outflow A, and seventy spectra were averaged toward Outflow B.

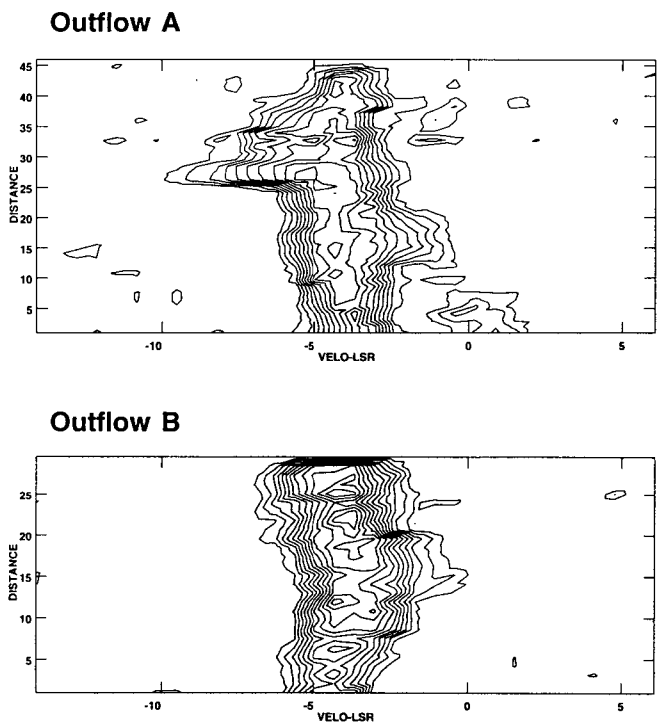

Fig. 11. The ^{12}CO position-velocity contour map for two outflows, A and B. The lowest contour and the increment between the contour levels are 0.4 K.

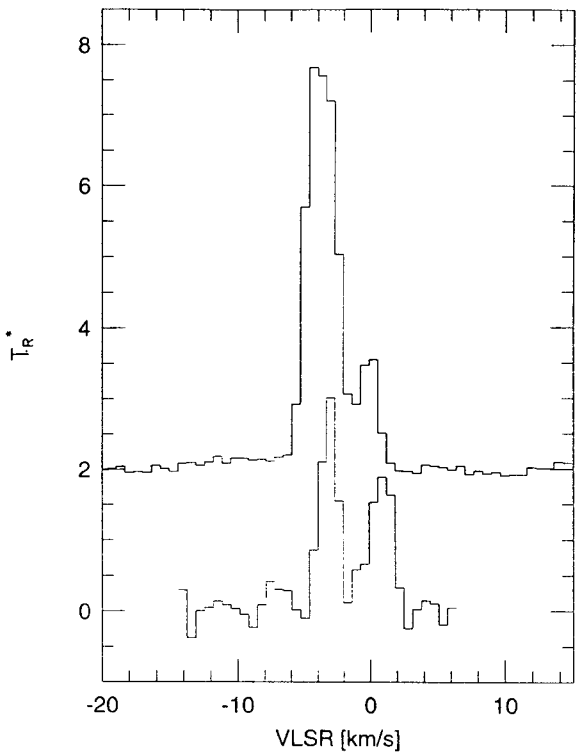

Fig. 12. The ^{12}CO line profiles toward two positions of 'Stripe'. The coordinate of lower spectra is $\alpha = 22^h25^m25^s, \delta = 74°40'$. The coordinate of upper spectra which is obtained in high sensitivity using DRAO 14 m telescope is $\alpha = 22^h27^m29^s.4, \delta = 74°50'$.

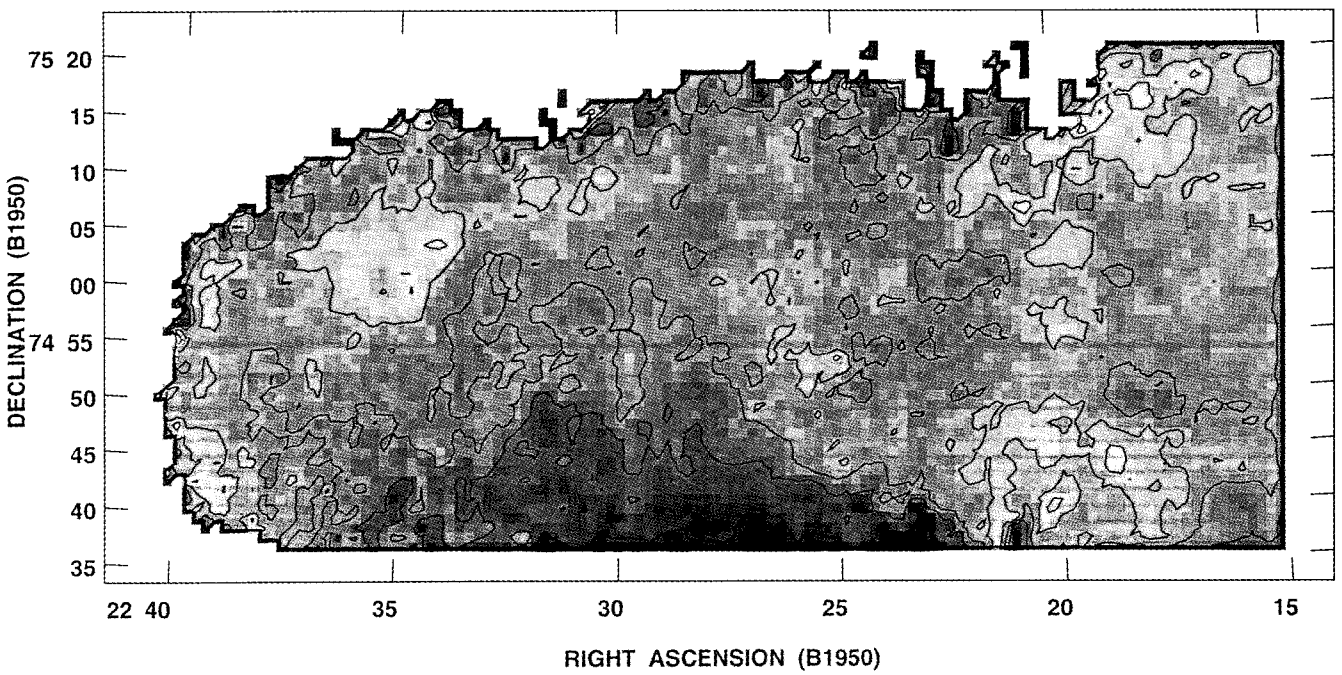

Fig. 13. The ^{12}CO linewidth map of L1251. The darker color represent the larger linewidth. The lowest contour is 1.5 km s^{-1}, and the increment between the contours is 0.75 km s^{-1}.

km s^{-1}. A map of mean velocity of the cloud is shown in Figure 8, and demonstrates that the cloud has some velocity field (the darker color, the more blueshifted); the lower part of the cloud is blueshifted mainly because of the 'Stripe', and the position centered on IRAS 22343+7501 shows blueshifted velocity. The mean velocity of L1247 (right-hand portion of the cloud) shows no conspicuous velocity gradient. All the mean velocity is demonstrated above a threshold integrated intensity, 2 K km s^{-1}.

(b) Mass Estimate

i) LTE Mass

A technique that has been widely used to estimate clouds masses is the LTE method. More detailed discussion of this technique and assumption inherent in its use can be found in many papers (Lee 1992; Lee *et al.* 1994; Dickman 1978). When both ^{12}CO and ^{13}CO lines have been observed toward each line of sight, the ^{13}CO column density can be determined. As a correlation between the visual extinction and ^{13}CO column density for L1251 has not been established, we should use a known correlation which was established for a set of normal dark cloud in the solar neighborhood. The validity of LTE technique should be checked before using this technique to estimate the cloud mass. However, especially for a cloud with large linewidths and high density it is known that the technique has been successful (Lee 1992).

The column density of ^{13}CO in the i-th pixel of a cloud is given:

$$N(^{13}CO)_i = \frac{2.42 \times 10^{14} \Delta V_i \, T_{ex} \, \tau^{13}}{1 - \exp[-5.29/T_{ex}]} [\mathrm{cm}^{-2}], \tag{1}$$

where ΔV_i is the full width at half-intensity in km s^{-1}, τ^{13} is the line center optical depth of ^{13}CO, and T_{ex} is the excitation temperature;

$$\tau^{13} = -\ln\left[1 - \frac{T_R^{13}}{\frac{5.29}{e^{5.29/T_{ex}}-1} - 0.93}\right], \tag{2}$$

$$T_{ex} = \frac{5.53}{\ln\left[1 + \frac{5.53}{T_R^{12}+0.876}\right]}. \tag{3}$$

The above equation was used for all the pixels with emission in ^{13}CO greater than the 3 σ noise level. For pixels with emission weaker than the 3 σ noise level, we assumed optically thin emission and used the integrated intensity of ^{13}CO:

$$N(^{13}CO)_i = \frac{3.76 \times 10^{14}}{f_u} \int T_R^*(^{13}CO) \, dv \quad [\mathrm{cm}^{-2}], \tag{4}$$

where f_u is the fraction of ^{13}CO in the upper state ($J = 1$). We take $f_1 = .55$ assuming $T_{ex} = 5$ K, assuming a temperature of 2 to 3 K.

With the correlation of visual extinction and ^{13}CO column density (Dickman 1978), the LTE mass for L1251 is estimated to be 640 $M_\odot$.

ii) Virial Mass Estimate

If a molecular cloud is virialized (gravitationally bound, and has had enough time to be dynamically relaxed), then the partition of energy will be governed by the virial theorem. In that case, the virial mass is given by

$$M_{VIR} = \frac{3\alpha\sigma_{tot}^2}{2G} D, \tag{5}$$

where D is the cloud diameter and σ_{tot} is velocity dispersion of the cloud, which represents all forms of kinetic motion within the cloud. The constant α is order of unity and depends on the shape and density distribution of the cloud. Since clouds are irregularly shaped, it is not straightforward to define a cloud size. We adopt as a measure of the mean cloud diameter $D = \sqrt{(4A/\pi)}$, where A is the area (see more discussion in Lee 1992 and 1994b). Here

we define the area of the cloud to be that covered by all pixels with ^{12}CO integrated intensity greater than 5σ. The size of L1251 is then 5.5 pc assuming a distance of 300 pc (Kun and Prusti 1993).

The velocity dispersion of the cloud is estimated to be 1.4 km s^{-1} (internal velocity dispersion is 1.14 km s^{-1}, and centroid velocity dispersion is 0.79 km s^{-1}), thus, the estimated virial mass is 6×10^3 $M_\odot$ assuming a uniform density distribution ($\alpha = 1.6$).

iii) Mass from CO Luminosity

Another mass estimate can be obtained by using the empirical relationship between the CO integrated intensity and molecular hydrogen column density, or equivalently, the relationship between CO luminosity and mass. This relationship has been studied by a number of investigators and reviewed by Scoville and Sanders (1987). Usually the virial mass is used to calculate the conversion factor. In fact, if clouds are virialized, a relation between total CO luminosity and cloud mass can be theoretically demonstrated to exist (Dickman, Snell, and Schloerb 1986). Empirical estimates of the conversion constant based on molecular observations vary between 1 and 5×10^{20} cm^{-2} (K km s^{-1})$^{-1}$ (Scoville and Sanders 1987).

The conversion factor has also been established through γ-ray analysis. Several γ-ray studies (Lebrun *et al.* 1983; Bloemen *et al.* 1984; and summary by Bloemen 1989) found similar conversion constant ranging from 2 to 3×10^{20} cm^{-2} (K km s^{-1})$^{-1}$. Also, the γ-ray analysis suggests that the conversion factor is roughly constant as a function of Galactic radius, except possibly for the center of the Galaxy (Bloemen 1987). One merit of this method for determining the conversion function is that it is independent of virial mass estimates; the γ-ray flux directly probes the hydrogen column density.

The ^{12}CO luminosity of L1251 is 270 K km s^{-1}. Thus, if we use the most recent estimate of the conversion factor established through γ-ray analysis, 2.3×10^{20} cm^{-2} (K km s^{-1})$^{-1}$ pc^{-2} (Bloeman 1989), we obtain a mass of 1,300 $M_\odot$.

(c) Two Bipolar Outflows

We have identified high-velocity ^{12}CO emission wing toward two IRAS point sources, IRAS 22343+7501 and IRAS 22376+7455, and confirmed that these are the bipolar outflows which were also studied by Sato and Fukui (1989, 1994) using Nagoya 4 m telescope (FWHM = 2'.7). The contour maps of two bipolar outflows are presented on the plate 1 (Figure 9) superposed on the 100 μm flux color image. The contours represents the two wing components (dashed line is red wing, and solid one is blue wing). The wings extend from -10 to 0 km s^{-1} in the velocity range. The contours of blue wings are the ^{12}CO integrated intensity between -10 and -6 km s^{-1}, and contours of red wings are between -2 and 0 km s^{-1}. Though the red wing component of a bipolar outflow centered on IRAS 22343+7501 (hereafter Outflow A; $V_{\rm LSR} = -10$ to 0 km s^{-1}) is contaminated by the emission of 'Stripe' (see previous section)', the contribution of 'Stripe' seems to be negligible comparing the major wing emission. Figure 9 indicates that the molecular gas in the wing components shows a clear bipolarity. The bipolar outflows are located on the exactly center of the two IRAS point sources, suggesting that these two point sources are driving two outflows. Bipolar outflow centered on IRAS 22376+7455 (hereafter Outflow B; $V_{\rm LSR} = -7.5$ to 0 km s^{-1}) has a highly-collimated bipolarity, and has a much larger blue-wing component than red wing component. It is also located at one of the densest part of the cloud (see above). These facts are implying that the bipolar outflow centered on the IRAS 22376+7455 is deeply embedded, and possibly close to the backside of the cloud.

In Figure 10 averaged profiles centered on two bipolar outflows are presented. One hundred and thirty (^{12}CO and ^{13}CO each) spectra were averaged toward Outflow A, and seventy spectra were averaged toward Outflow B. The averaged ^{12}CO spectra show blue and red wings ranging -8 to 0 km s^{-1} both for Outflows A and B, though the red wing of Outflow B is very weak. The blue wing component of Outflow B seems to be contaminated with the emission of the 'Stripe', thus it does not show clear wing. Figure 11 is the spatial velocity contour maps toward two outflows: Outflow A shows very clear wings and the part of the 'Stripe' appears at the bottom of the map. It is remarkable that the red wing of Outflow B is very weak comparing with its blue wing component. Both the contour maps are obtained along the their collimated axes.

The far-infrared luminosities are calculated for these two outflows using the following equation (Lonsdale *et al.* 1985):

$$L_{FIR} = 4\pi d^2[1.26R(1.00 \times 10^{12} S_{100} + 2.58 \times 10^{12} S_{60})], \quad (6)$$

where S_ν is the flux density at IRAS band ν, d is the distance to the object, and R is the color correction factor. For IRAS 22343+7501 the flux density at 100 μm is 80.04 Jy, and at 60 μm 66.34 Jy. For IRAS 22376+7455 it is 66.84 at μm, and 32.34 Jy. The color correction factor R is adopted from the definition of IRAS Supplementary (Lonsdale *et al.* 1985); 1.2 for IRAS 22343+7501, and 1.38 for IRAS 22376+7455. Luminosities were obtained assuming that the distance of IRAS point sources is 300 pc. We obtained $L_{FIR} = 10.5 L_\odot$ for IRAS 22343+7501, and $7.2 L_\odot$ for IRAS 22376+7455.

IV. DISCUSSION

(a) Velocity Field and the 'Stripe'

L1251 has a very intriguing velocity field, if 'Stripe' cloud are really associated with the main cloud. Thus, we have to discuss the association possibility of two clouds.

There are two facts which may favor the association possibility. First, there is a possible connection sign in the position-velocity map (Figure 7). Spectra shows also the same sign for at least 20′. Second, there is clear velocity gradient in the 'Stripe' cloud. The amount of gradient is about 0.3 km s^{-1} pc^{-1} along the cloud.

If the 'Stripe', the higher velocity component, is really associated with the main cloud, and this velocity pattern matches what would be expected for an expanding shell, an dynamical age of the "Stripe" can be estimated. The angular size of the 'Stripe' is about 1 degree, which is corresponding to 5 pc, and expansion velocity of 3 or 4 km s^{-1} is suggesting a dynamical age of about 10^6 years.

However, there are also unfavorable clues: the most critical one is that there is no systematic velocity field in the main cloud L1251. The velocity is fairly stable over the whole extent of the cloud except the two outflows region. Except these two there is no internal or external driving source identified. If there is any driving source, such as strong stellar wind, the main cloud should be disturbed severely. For example, the velocity structure of a molecular cloud associated with an HII region S287 and other external driving sources such as strong stellar winds (Lee 1994b) shows several arcs, and filamentary components. The size and mass of S287 molecular cloud are much larger than those of L1251. Thus, if there are any driving sources, the cloud morphology should be more disturbed. There is no such sign in the main cloud of L1251.

The ^{12}CO line profiles toward two positions of 'Stripe' are shown in Figure 12. The coordinate of lower spectra is $\alpha = 22^h25^m25^s, \delta = 74°40'$. The coordinate of upper spectra which is obtained using DRAO 14 m telescope is $\alpha = 22^h27^m29^s.4, \delta = 74°50'00''$. The spectra themselves do not give a key to answer whether two clouds are associated. While the mean velocity of the main cloud is rather stable, the mean velocity of the 'Stripe' shows a clear gradient. This may strengthen the clue that the small 'Stripe' has some velocity field, and that it is just superposed on L1251. Figure 13 shows the linewidths map toward all the pixels mapped. The darker color represents broader linewidth. The linewidths of two outflows are the most outstanding ones as expected. The 'Stripe' linewidths is inevitably large as two lines are possibly superposed toward this region. Thus, we preferred the later case, namely, the 'Stripe' cloud does not seem to be associated with the main cloud.

If the 'Stripe' is not associated with the main cloud, L1251 is rather quiescent cloud. The only sources that effect the dynamics of the gas are two outflows, which are preferentially located on the head of the cigar-shaped cloud. Sato and Fukui (1994) estimated the total kinematic energy of Outflow A to be 12% of turbulence energy of their cores, and the kinematic energy of Outflow B is $\sim$ 2%. Thus, the Outflow A, which has a very extended wing structure, seems to be influencing significantly on the dynamics of L1251, though it is not enough to reshape the whole extent of the cloud.

Sato and Fukui (1994) claimed that the head part of the cloud is U-shaped, and this structure maybe resulted from some dynamical interaction with ambient matter, and discarded the possibility that the supernova remnant caused the U-shaped structure. However, their velocity gradient estimated toward this region was not confirmed in our study. We presented the mean velocity map in Figure 8, in which the velocity field toward this region is

dominated by two outflows. This fact was also confirmed by the spatial-velocity map presented in Figure 7. The gradient detected may be resulted from contamination of 'Stripe' component and two bipolar outflows.

(b) Bipolar Outflows

The bipolar outflows A and B are matching with the most bright IRAS point sources, IRAS 22343+7501 and 22376+7455, which are the driving sources. The estimated far-infrared luminosities of these two IRAS point sources are lower bounds of typical luminosities of T Tauri stars. This implies that the embedded objects are low-mass objects just passed the protostellar stage. In fact, though there is no stellar counterpart on the POSS print, Balázs *et al.* (1992) identified several knots which might be Herbig-Haro objects, and Kun and Prusti (1993) identified many low-mass T Tauri stars and Hα stars toward these two outflows.

According to Sato and Fukui (1989), the interstellar gas around IRAS 22343+7501 has been exhausted to form a newly born star and/or that the outflow has disrupted the dense clump as the point source lies in the marginal area of the dense core.

The maximum extent of Outflow A is $\sim$ 30' along its axis, and it is corresponding to 2.6 pc, assuming a distance of 300 pc. Thus, the dynamical time scale of Outflow A is estimated to be $\sim 2.5 \times 10^5$ yr from the velocity extent of 10 km s^{-1}. The maximum extent of Outflow B is $\sim$ 15' along its axis, and it is corresponding to 1.3 pc. The dynamical time scale of Outflow B is thus, estimated to be $\sim 1.7 \times 10^5$ yr from the velocity extent of 8 km s^{-1}. The estimated dynamical time scale of the two bipolar outflows is a factor of two different from the estimate of Sato and Fukui (1989). The difference is caused by mainly the distance determination, and their estimate of spatial extent is a bit underestimated as they use much larger beam.

(c) Physical Properties

i) Mass Determination

The cloud mass has been estimated in three different ways. The LTE estimate (640 $M_\odot$) is the smallest and the virial estimate (6×10^3 $M_\odot$) is the largest. Incredably, the difference between the largest and smallest estimate is a factor of 10. The virial estimate is very huge for a quiescent cloud like L1251. In fact, the cloud is not likely to be virialized as is the usual case for dark cloud. According to Maloney (1988), the existence of turbulence throughout the interstellar medium suggests that an appropriate value for the average pressure may be P/k larger than about 10,000. He introduced negative-index polytropic models of interstellar clouds in equilibrium with an external medium at these pressures, and predicted their sizes, line widths, masses, and size-line width and size-density relations in good agreement with those observed and inferred for dark clouds. Thus, these observed features of interstellar clouds do not require that they be completely self-gravitating or 'virialized' in commonly used sense. This is applied only for small clouds, such as dark clouds. In fact, the virial estimate of L1251, a quiescent cloud, is much larger than other two estimates, and the internal velocity dispersion, 1.2 km s^{-1}, is significantly larger than that of centroid velocity dispersion, 0.8 km s^{-1}, and almost comparable with that of some GMCs (Scoville *et al.* 1987). Although there are some uncertainties determining the parameters, such as size and density model of the clouds, these are all within 20 to 30 percent of the estimate. Thus, we discard the possibility of virial equilibrium of L1251 and its mass estimate.

As is usual, the LTE mass estimate is the smallest. This point has been discussed in many other papers (Lee, Snell, and Dickman 1990; Lee 1994b). LTE mass estimate might significantly miss the mass outside the cloud boundary, and it is based on several critical assumptions. However, the LTE estimate is found quite reliable if the relationship between ^{13}CO column density and visual extinction is established (Lee 1992; Lee *et al.* 1994). Lee (1992) found that the intercept of the relation between ^{13}CO column density and visual extinction should be included to compensate the mass outside the boundary. However, the relationship between ^{13}CO column density and visual extinction has not been established, and we used a ^{13}CO abundance obtained by Dickman (1978). Thus, the LTE mass is quite underestimated within 50 to 100%.

The mass estimated using universal conversion factor endows us a quite reasonable value, 1.3×10^3 $M_\odot$ comparing with LTE estimate. The existence of a general relation between mass and CO luminosity may be the result of most clouds being in virial equilibrium. If G216-2.5 is not in virial equilibrium, its mass could be overestimated by this

technique (Lee *et al.* 1994).

Overall, a factor of two or even three difference between mass estimates could easily be attributed to a combination of the uncertainties mentioned above. As discussed above paragraph, assuming the LTE mass estimate is a lower limit and mass estimate using CO integrated intensity is an upper limit, we can take the cloud mass as the average of two estimate. Hence, 1000 $M_\odot$ is taken as the mass of the L1251.

ii) Density

Taking a total mass of L1251 as 10^3 solar masses, we can estimate the volume density of the cloud. The length was estimated to 8 pc and the width was 4 pc. The third axis of the cloud is unknown, however, it should not be much larger or smaller than other axes. Thus, we take the length of third axis as the average of other two axes, 6 pc. Thus, the volume density was estimated to be order of hundred per cubic centimeter. The average volume density of dark clouds in solar neighborhood ranges from hundred to few thousand per cubic centimeter. Thus, the volume density estimated is rather smaller side of the density range of dark clouds.

V. Summary

We have mapped the whole extent of a dark cloud Lynds 1251 in the emission of the $J = 1 - 0$ transitions of ^{12}CO and ^{13}CO using FCRAO's fifteen-beam array receiver in high resolution of 50″.

We summarize the results of present study as follow:

1. We have discussed three different mass estimates, and obtained a large range of mass, 600 to 6,000 $M_\odot$, depending on the technique. The factor of 10 discrepancy between the virial and LTE masses is much larger than expected based on the uncertainties in two methods. The large viral mass may reflect the fact that L1251 is not gravitationally bound system as in the case of dark clouds in solar neighborhood.

2. Two outflows are affecting the dynamics of cloud significantly but not enough to reshape the whole extent of the cloud.

3. The 'apparently-associated Stripe' is not likely to be connected with the main cloud L1251. The velocity gradient composed on this small cloud may be driven by other unknown small scale sources.

4. The cloud itself is very quiescent except the two bipolar outflow regions. There is no systematic velocity field found toward L1251.

ACKNOWLEDGEMENTS

This research has been supported by Korea Astronomy Observatory's Basic Research Fund Program.

REFERENCES

Balazs, L.G., Eisloffel, J. Holl, A., Kelemen, J., and Kun, M., 1992,*A.A.*, 255, 281.

Bloemen, J. B. G. M. 1987, in *Interstellar Process*, eds. D. J. Hollenbach and H. A. Thronson, Jr. (Dordrecht: Reidel), p. 143.

Bloemen, J. B. G. M. 1989, *ARAA*, 27, 469.

Bloemen, J. B. G. M., Caraveo, P. A., Hermsen, Lebrun, F., Maddalena, R. J., Strong, A. W., and Thaddeus, P. 1984, *AA*, 139, 37.

Dickman, R. L. 1978b, *AJ*, 83, 363.

Dickman, R. L., Snell, R. L., and Schloerb, F. P. 1986, *ApJ*, 306, 326.

Fuller, G.A. 1989, Ph.D. Dissertation, University of California, Berkeley.

Fukui, Y. 1989, in *ESO Workshop No. 33; Low Mass Star Formation and Pre-main Sequence Objects*, ed. B. Reipurth, p. 95.

Grenier, I.A., Lebrun, F., Arnaud, M., Dame, T.M., and Thaddeus, P. 1989, *ApJ*, 347, 231.

Kun, M. and Prusti, T. 1993, *A.A.*, 272, 235.

Kutner, M. C., and Ulich, B. L. 1981, *ApJ*, 250, 341.
Lebrun, F., Bennet, K., Bignami, G., Bloemen, J. B. G. M., Bucherri, R., 1983, *ApJ*, 281, 634.
Lee, Y., Snell, R. L., and Dickman, R. L. 1990, *ApJ*, 355, 536.
Lee, Y., Snell, R.L., Dickman, R.L. 1994, *ApJ*, 432, 167.
Lee, Y. 1992, Ph. D. Dissertation, University of Massachusetts.
Lee, Y. 1994a, in preparation (Paper II)
Lee, Y. 1994b, in press, Publication of Korean Astronomical Society.
Lee, Y. 1994c, in press, Journal of Korean Astronomical Society.
Lonsdale, G., Helou, G., Good, J. C., and Rice, W. 1985, *Catalogued Galaxies and Quasars Observed in the IRAS Survey* (Pasadena: Jet Propulsion Laboratory).
Lynds, B.T. 1962, *ApJ*, 7, 1.
Lynds, B.T. 1965, *ApJ*, 12, 163.
Maloney, P. 1988, *ApJ*, 334, 761.
Sanders, D.B., Scoville, N.Z., Tilanus, R.P.J., Wang, Z, and Zhou, S. 1993, AIPS Conference Proceedings 278, *Back to the Galaxy*, eds. Holt, S.S., and Verter, F. American Institute of Physics, p331.
Sato, F. and Fukui, Y., 1989, *ApJ*, 343, 773.
Sato, F. and Fukui, Y., 1989, *ApJ*, 343, 773.
Scoville, N. Z., and Sanders, D. B. 1987, in *Interstellar Processes*, eds. D. J. Hollenbach and H. A. Thronson, Jr., p. 21.
Scoville, N. Z., Yun, M. S., Clemens, D. P., Sanders, D. B., and Waller, W. H. 1987, *ApJS*, 63, 821.